



OPTIMIZATION OF SLOPE CRITICAL SURFACES USING SA_EVPS ALGORITHM WITH SEEPAGE AND SEISMIC EFFECTS

M. Paknahad¹, P. Hosseini^{1*,†}, A.R. Mazaheri², and A. Kaveh³

¹*Faculty of Engineering, Mahallat Institute of Higher Education, Mahallat, Iran*

²*Faculty of Engineering, Ayatollah Borujerdi University, Borujerd, Iran*

³*Center of Excellence for Fundamental Studies in Structural Engineering, School of Civil Engineering, Iran University of Science and Technology, Tehran-16, Iran*

ABSTRACT

This study presents a novel approach for optimizing critical failure surfaces (CFS) in homogeneous soil slopes by incorporating seepage and seismic effects through the Self-Adaptive Enhanced Vibrating Particle System (SA_EVPS) algorithm. The Finite Element Method (FEM) is employed to model fluid flow through porous media, while Bishop's simplified method calculates the Factor of Safety (FOS). Two benchmark problems validate the proposed approach, with results compared against traditional and meta-heuristic methods. The SA_EVPS algorithm demonstrates superior convergence and accuracy due to its self-adaptive parameter optimization mechanism. Visualizations from Abaqus simulations and comprehensive statistical analyses highlight the algorithm's effectiveness in geotechnical engineering applications. The results show that SA_EVPS consistently achieves lower FOS values with smaller standard deviations compared to existing methods, indicating more accurate identification of critical failure surfaces.

Keywords: Slope stability; Critical failure surface; SA_EVPS algorithm; Meta-heuristic optimization; Geotechnical engineering.

Received: 29 April 2025; Accepted: 3 July 2025

*Corresponding author: Faculty of Engineering, Mahallat Institute of Higher Education, Mahallat, Iran
P.Hosseini@mahallat.ac.ir (P. Hosseini)

1. INTRODUCTION

Slope stability analysis represents a fundamental challenge in geotechnical engineering, essential for ensuring the safety and reliability of infrastructure including embankments, dams, and highways. The primary objective involves identifying the Critical Failure Surface (CFS) and its associated Factor of Safety (FOS), which quantifies a slope's resistance to failure under various loading conditions. Early analytical methods relied primarily on manual calculations, significantly limiting their applicability to simple geometries and idealized conditions. The development of computational techniques, particularly Limit Equilibrium Methods (LEMs) pioneered by Fellenius [1], Bishop and Morgenstern [2], Morgenstern and Price [3], and Spencer [4], revolutionized slope stability analysis by enabling more complex analyses. However, LEMs often assume simplified failure surface geometries (typically circular) and encounter difficulties when addressing complex loading conditions, particularly those involving seepage and seismic forces [5].

Seepage fundamentally alters the stress distribution within slopes by modifying pore water pressure, consequently reducing effective stress and potentially triggering instability. Similarly, seismic forces introduce dynamic loads that can dramatically reduce slope stability through cyclic loading and excess pore pressure generation. Accurate modeling of these coupled effects requires sophisticated numerical methods such as the Finite Element Method (FEM), which solves the governing differential equations of fluid flow and stress distribution simultaneously. Traditional optimization methods, including grid search, simplex, and conjugate-gradient techniques, have been extensively applied to locate the CFS [6,7]. While these deterministic methods offer robustness in certain applications, they suffer from high computational costs and susceptibility to convergence at local minima in non-convex solution spaces, particularly when evaluating multiple trial failure surfaces [8].

Meta-heuristic algorithms have emerged as powerful alternatives to address these computational limitations by efficiently exploring complex, multi-dimensional solution spaces. These algorithms, inspired by natural phenomena or mathematical principles, include Genetic Algorithms (GA) [9], Particle Swarm Optimization (PSO) [10], and Firefly Algorithm (FA) [11], all of which have demonstrated success in slope stability problems. However, their performance typically depends on manually tuned parameters that may not be optimal across different problem types [12]. This limitation can result in inconsistent performance and necessitates extensive parameter sensitivity analyses.

The Self-Adaptive Enhanced Vibrating Particle System (SA_EVPS) algorithm, recently introduced by Paknahad et al. [13], addresses this fundamental limitation through dynamic parameter optimization tailored to each specific problem [14]. Building upon the foundation of the Enhanced Vibrating Particle System (EVPS) [15], SA_EVPS incorporates a self-adaptive mechanism that optimizes its internal parameters before the main optimization process. This innovation enhances both convergence speed and solution quality, making it particularly suitable for complex geotechnical optimization tasks. The SA_EVPS and EVPS algorithms have already demonstrated their versatility through successful applications in various engineering domains, including optimization of large-scale truss structures [16], concrete mix design optimization using artificial neural networks [17-19], and reliability-based design optimization [20].

This study applies the SA_EVPS algorithm to optimize the CFS of homogeneous soil

slopes while comprehensively accounting for seepage and seismic effects through FEM integration. Two well-established benchmark problems, previously analyzed by Malkawi et al. [21] and Zolfaghari et al. [9], serve to validate the proposed approach through rigorous comparison with existing methods.

The primary motivation for employing SA_EVPS lies in its ability to adaptively tune parameters, thereby reducing reliance on empirical adjustments and improving robustness across diverse problem configurations. The seamless integration of FEM ensures accurate modeling of seepage-induced pore pressures and seismic forces, significantly enhancing the reliability of FOS calculations. This paper contributes to the geotechnical engineering field by demonstrating SA_EVPS's superior efficacy in slope stability optimization and establishing a comprehensive framework for future applications.

The remainder of this paper is organized as follows: Section 2 presents the mathematical formulation of fluid flow equations and their FEM implementation. Section 3 describes the SA_EVPS algorithm architecture and the formulation of the objective function. Section 4 presents the benchmark problems, computational results, and comparative analyses. Section 5 provides a critical analysis of SA_EVPS performance, limitations, and potential improvements. Section 6 concludes with key findings and directions for future research.

2. FLUID FLOW THROUGH POROUS MEDIA

2.1 Strong Form of the Governing Equation

Fluid flow through porous media, such as saturated soil, is governed by Darcy's law, which establishes a linear relationship between fluid velocity and hydraulic gradient. For a two-dimensional domain, the continuity equation, when combined with Darcy's law, yields the strong form of the governing equation as Eq.(1):

$$\frac{\partial}{\partial x} \left(k_x \frac{\partial \phi}{\partial x} \right) + \frac{\partial}{\partial y} \left(k_y \frac{\partial \phi}{\partial y} \right) + Q = 0 \quad (1)$$

where ϕ represents the fluid head (m), k_x and k_y denote the permeability coefficients (m/s) in the x and y directions respectively, and Q represents the volumetric flow rate per unit volume S^{-1} . The boundary conditions for this problem include:

- Dirichlet boundary condition: $\phi = \bar{\phi}$ on surface Γ_q
- Neumann boundary condition: $k_x \frac{\partial \phi}{\partial x} n_x + k_y \frac{\partial \phi}{\partial y} n_y = \bar{q}$ on surface Γ_q

where n_x and n_y represent the direction cosines of the outward normal to Γ_q , and \bar{q} denotes the prescribed flux across the boundary.

2.2 Weak Form Derivation

To implement the FEM, the strong form must be transformed into its weak form by introducing a test function w and integrating over the domain Ω :

$$\int_{\Omega} w \left[\frac{\partial}{\partial x} \left(k_x \frac{\partial \phi}{\partial x} \right) + \frac{\partial}{\partial y} \left(k_y \frac{\partial \phi}{\partial y} \right) + Q \right] d\Omega = 0 \quad (2)$$

Applying integration by parts and utilizing the divergence theorem, the weak form becomes:

$$\int_{\Omega} \left[k_x \frac{\partial w}{\partial x} \frac{\partial \phi}{\partial x} + k_y \frac{\partial w}{\partial y} \frac{\partial \phi}{\partial y} \right] d\Omega - \int_{\Gamma} w \left(k_x \frac{\partial \phi}{\partial x} n_x + k_y \frac{\partial \phi}{\partial y} n_y \right) d\Gamma + \int_{\Omega} w Q d\Omega = 0 \quad (3)$$

The boundary integral is subsequently simplified using the Neumann boundary condition, resulting in a formulation suitable for FEM discretization.

2.3 Finite Element Formulation

The computational domain is discretized into three-node triangular elements for numerical efficiency. Within each element, the fluid head is approximated using shape functions:

$$\phi^e = \sum_i N_i \phi_i \quad (4)$$

where N_i represent the shape functions and denote the nodal fluid head values. For a triangular element, the shape functions are expressed as:

$$N_i = \frac{a_i + b_i x + c_i y}{2A} \quad (5)$$

where A represents the element area, and the coefficients a_i , b_i , are computed from nodal coordinates using standard finite element procedures. . The gradient matrix \mathbf{B} is formulated as:

$$\mathbf{B} = \begin{bmatrix} \frac{\partial N}{\partial x} \\ \frac{\partial N}{\partial y} \end{bmatrix} \quad (6)$$

The velocity field is subsequently related to the gradient through:

$$\mathbf{v} = -\mathbf{D}\nabla\phi = -\mathbf{D}\mathbf{B}\phi \quad (7)$$

where \mathbf{D} represents the permeability matrix. The element stiffness matrix is computed as:

$$\mathbf{K}^e = \int_{\Omega^e} \mathbf{B}^T \mathbf{D} \mathbf{B} d\Omega^e \quad (8)$$

where the integration is performed over the element domain. The force vector incorporates contributions from volumetric sources Q and boundary fluxes. Solution of the global system $\mathbf{K}\phi = \mathbf{F}$ yields the fluid head distribution throughout the domain, which is subsequently used to compute pore pressures using the relationship $u = \gamma_w \phi$.

3. SLOPE STABILITY OPTIMIZATION USING SA_EVPS

3.1 SA_EVPS Algorithm

The SA_EVPS algorithm represents a significant advancement over the Enhanced Vibrating Particle System (EVPS) through its incorporation of dynamic parameter optimization. Unlike EVPS, which utilizes fixed parameters (typically $\alpha = 0.05$, $p = 0.2$), SA_EVPS employs a preliminary optimization phase to determine optimal values for all algorithm parameters (α , p , w_1 , w_2 , HMCR, PAR, Neighbor, Memory_size) [22]. This self-adaptive mechanism ensures robust performance across diverse problem types without requiring manual parameter tuning.

$$x_i^j = x_{\min} + \text{rand} \cdot (x_{\max} - x_{\min}) \quad (9)$$

The damping factor, crucial for balancing exploration and exploitation, is updated iteratively according to:

$$D = \left(\frac{\text{iter}}{\text{iter}_{\max}} \right)^{-\alpha} \quad (10)$$

The weight coefficients, which control the influence of different solution components, satisfy the constraint:

$$w_1 + w_2 + w_3 = 1 \quad (11)$$

New positions are computed based on three reference points: the best historical position (OHB), the global best position (GP), and the best particle position (BP). This multi-reference approach ensures comprehensive exploration of the solution space while maintaining convergence toward promising regions [22]. The EVPS algorithm has demonstrated its effectiveness in various engineering applications, including discrete optimization problems [23].

3.2 Objective Function

The Factor of Safety (FOS) is calculated using Bishop's simplified method, which provides an optimal balance between computational efficiency and accuracy. For a circular failure surface divided into n vertical slices, the FOS is expressed as:

$$\text{FOS} = \frac{\sum_{i=1}^n \left[\frac{c'b_i + (W_i - u_i b_i) \tan \phi'}{m_{ai}} \right]}{\sum_{i=1}^n [W_i \sin \alpha_i + k_h W_i \cos \alpha_i]}, m_{ai} = \cos \alpha_i + \frac{\sin \alpha_i \tan \phi'}{\text{FOS}} \quad (12)$$

where:

- c' represents the effective cohesion (kPa)
- ϕ' denotes the effective friction angle (degrees)
- $W_i = \gamma h_i b_i$ represents the weight of slice i
- $u_i = \gamma_w \phi_i$ represents the pore pressure from FEM analysis
- b_i denotes the width of slice base
- α_i represents the inclination angle of slice base
- $k_h W_i$ represents the horizontal seismic force

The optimization problem is formally stated as:

$$\begin{aligned} &\text{Minimize: FOS}(x_c, y_c, R) \\ &\text{Subject to: Geometric constraints ensuring valid failure surfaces} \end{aligned} \quad (13)$$

The constraints ensure that the failure surface intersects the slope geometry appropriately and maintains physical validity throughout the optimization process.

The complete optimization procedure for determining the critical failure surface using the SA_EVPS algorithm is illustrated in the flowchart presented in Figure 1. This flowchart demonstrates the systematic approach from initial parameter optimization through convergence to the final critical failure surface identification.

4. NUMERICAL EXAMPLES

4.1 Benchmark Problem I

This benchmark problem, originally analyzed by Malkawai et al. [21], is a well-established test case in slope stability literature due to its simplicity and ability to challenge optimization algorithms. It involves a homogeneous soil slope with:

$$\text{Effective cohesion: } c' = 9.8 \text{ kN/m}^2, \quad \text{Friction angle: } \phi' = 10^\circ, \quad \text{Unit weight: } \gamma = 17.64 \text{ kN/m}^3$$

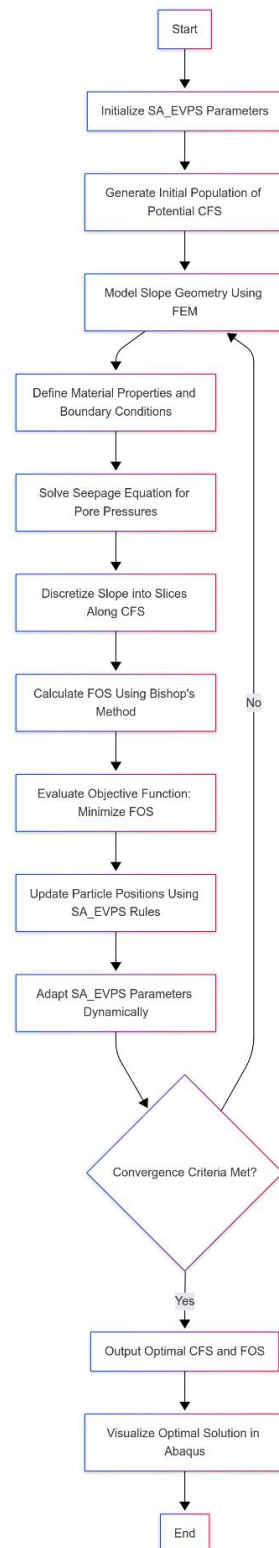


Figure 1: Flowchart of the SA_EVPS Algorithm for Slope Stability Optimization

The slope geometry, illustrated in Figure 2, features a height of 10 meters and an inclination angle of 26.57° . The slope extends 20 meters horizontally from the toe to the crest. The water table is positioned 2 meters below the crest, creating a seepage condition that influences pore water pressure distribution. Seismic effects are modeled using a horizontal seismic coefficient $k_h = 0.1$, simulating moderate earthquake loading.

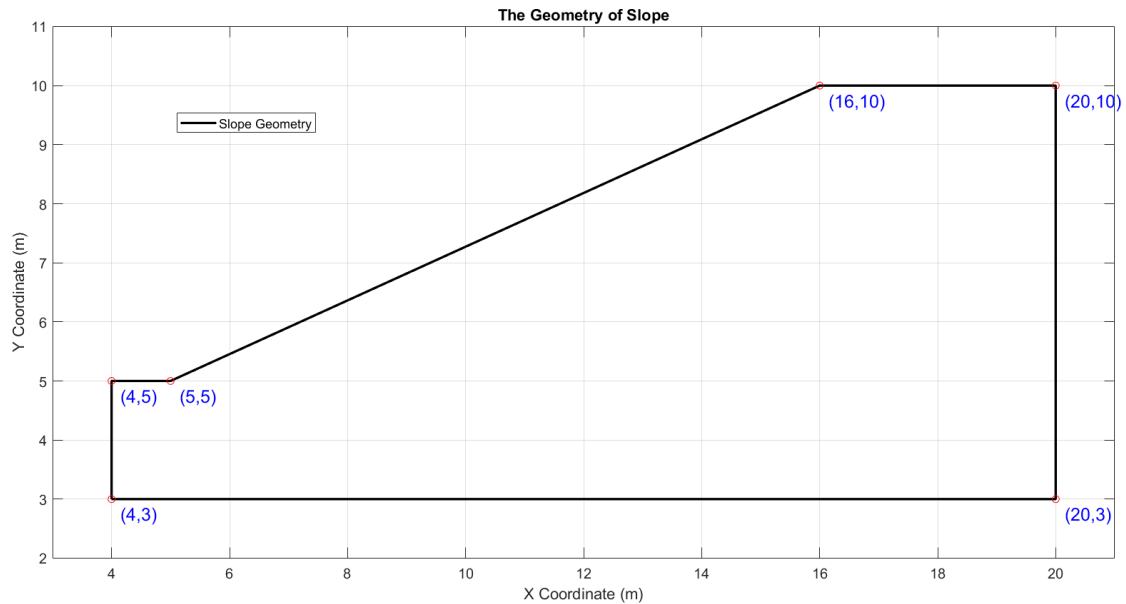


Figure 2: Geometry of Benchmark Problem I

The Finite Element Method (FEM) was employed to model fluid flow through the slope, using a mesh of 500 three-node triangular elements. The application of FEM in slope stability analysis, particularly using ABAQUS software, has been validated in previous studies examining the effect of soil parameters on earth dam slope stability [24]. Boundary conditions for seepage included a fixed head of 10 meters on the upstream face (left boundary) and a seepage face on the downstream slope, allowing water to exit freely. The FEM analysis provided pore water pressures, which were integrated into the stability calculations.

The SA_EVPS algorithm was configured with a population size of 40 particles, a maximum of 60 iterations, and 30 independent runs to ensure statistical reliability. The slope was divided into 20 vertical slices using the Fixed Slice Division Method (FSDM) for FOS calculations via Bishop's simplified method. The search space for the critical failure surface was defined with $x_c \in [0, 20]$ m, $y_c \in [5, 15]$ m, and $R \in [5, 15]$ m. Results are summarized in Table 1, showing the best FOS, average FOS, and standard deviation over the 30 runs.

The optimal CFS has coordinates $x_c = 8.552$ m, $y_c = 14.251$ m, and radius $R = 9.918$ m, yielding a minimum FOS of 1.2997. This FOS is notably lower than those reported in previous studies, indicating a more critical failure surface. The critical failure surface characteristics obtained from different optimization methods have been compared in Table 2.

Table 1: Statistical Results for Benchmark Problem I Using SA_EVPS

		BHMO	EFA	CMA-ES	ECM	SCA	Present study
Benchmark 1	Best	1.30E + 00	1.31E + 00	1.73E + 00	1.32E + 00	2.13E + 00	1.2997
	Average	1.30E + 00	1.31E + 00	2.17E + 00	1.33E + 00	2.85E + 00	1.3001
	Std.	9.20E - 14	4.28E - 03	5.75E - 01	2.41E - 02	4.69E - 01	1.77E-04

Table 2: Comparison of surface properties for Benchmark Problem I

CFS Properties	BHMO	EFA	CMA-ES	ECM	SCA	Present study
x Coordinate(m)	8.5962	8.5964	8.6080	8.5767	8.6624	8.552
y Coordinate(m)	14.1563	14.1325	14.1291	14.2398	14.1322	14.251
Radius(m)	9.8345	9.8320	9.8412	9.9175	9.8613	9.918

Comparisons with other optimization methods are presented in Table 3, highlighting SA_EVPS's superior performance.

Table 3: Comparison of FOS Values for Benchmark Problem I

Researcher	Method	Number of Slices	Limit Equilibrium Method	FOS
Yamagami and Veta [25]	BFGS	-	Morgenstern-Price Method	1.3380
Yamagami and Veta [25]	DFP	-	Morgenstern-Price Method	1.3380
Yamagami and Veta [25]	Powell	-	Morgenstern-Price Method	1.3380
Yamagami and Veta [25]	Nelder-Mead	-	Morgenstern-Price Method	1.3480
Greco [26]	Pattern Search	-	Spencer's Method	1.3300
Greco [26]	Monte Carlo	-	Spencer's Method	1.3330
Malkawai et al. [20]	Monte Carlo	-	Spencer's Method	1.2380
Cheng et al. [27]	PSO	20	Spencer's Method	1.3285
Kalatehjari et al. [10]	PSO	24	Bishop's Method	1.3128
Himanshu and Burman [28]	PSO	25	Bishop's Method	1.3141
Kaveh and Seddighian [29]	BHMO	20	Bishop's Method	1.3044
Kaveh and Seddighian [29]	EFA	20	Bishop's Method	1.3140
Kaveh and Seddighian [29]	CMA-ES	20	Bishop's Method	1.7289
Kaveh and Seddighian [29]	ECM	20	Bishop's Method	1.3207
Kaveh and Seddighian [29]	SCA	20	Bishop's Method	2.1335
Present study	SA_EVPS	20	Bishop's Method	1.2997

The critical failure surface is visualized in Figure 3, overlaid on the slope geometry, showing its position relative to the slope crest and toe.

Figure 4 presents the Abaqus simulation of the optimized state, displaying displacement contours along the slope. The maximum displacements are concentrated along the critical slip surface, confirming the accuracy of the SA_EVPS optimization in identifying the most vulnerable failure plane.

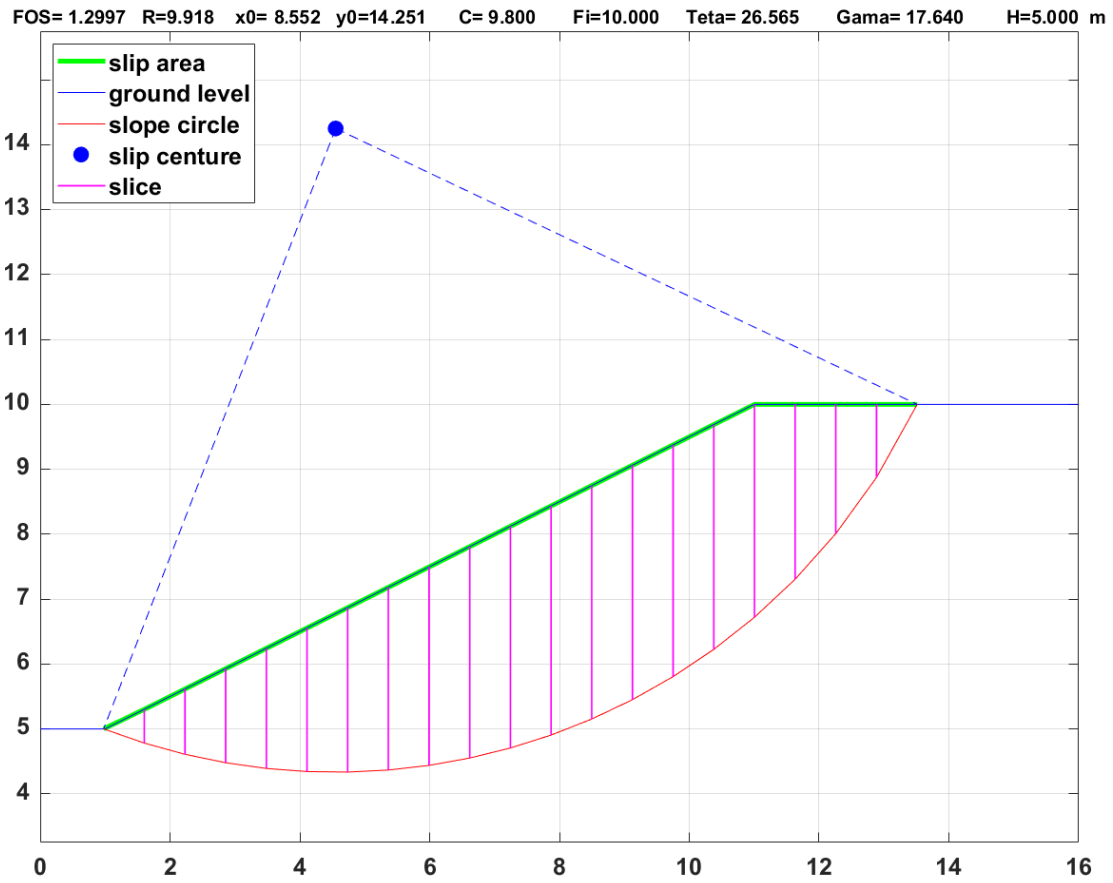


Figure 3: Critical Failure Surface for Benchmark Problem I

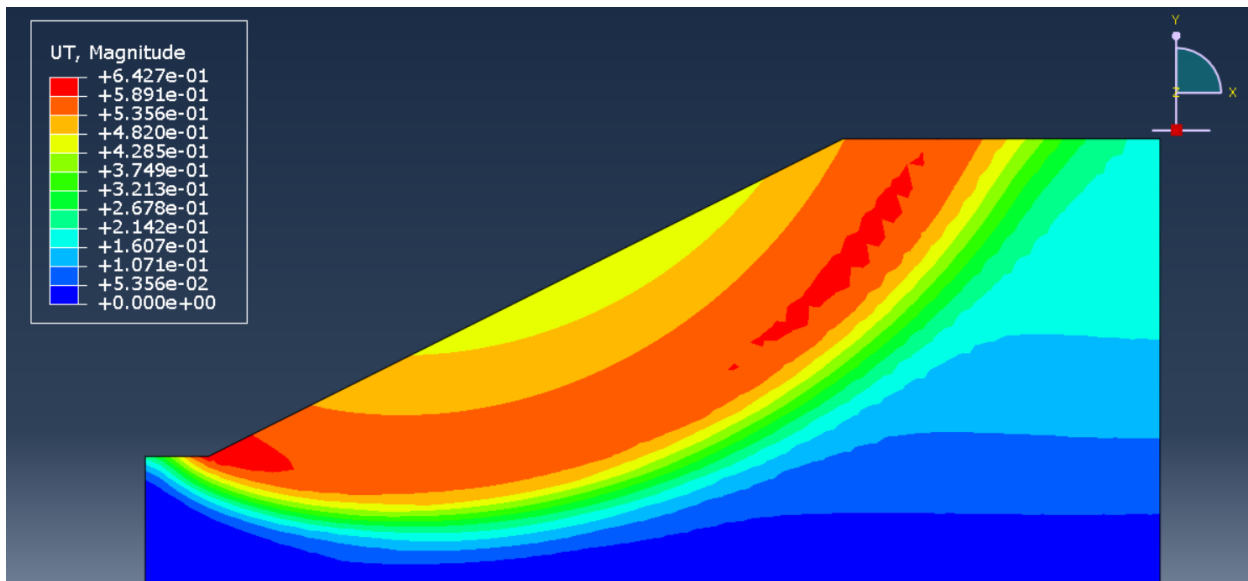


Figure 4: Abaqus Simulation of Optimized State for Benchmark Problem I

The convergence behavior of SA_EVPS is illustrated in Figure 5, which plots the FOS values over iterations for the 30 runs. The algorithm consistently converged to the minimum FOS within approximately 40 iterations, demonstrating its efficiency and robustness.

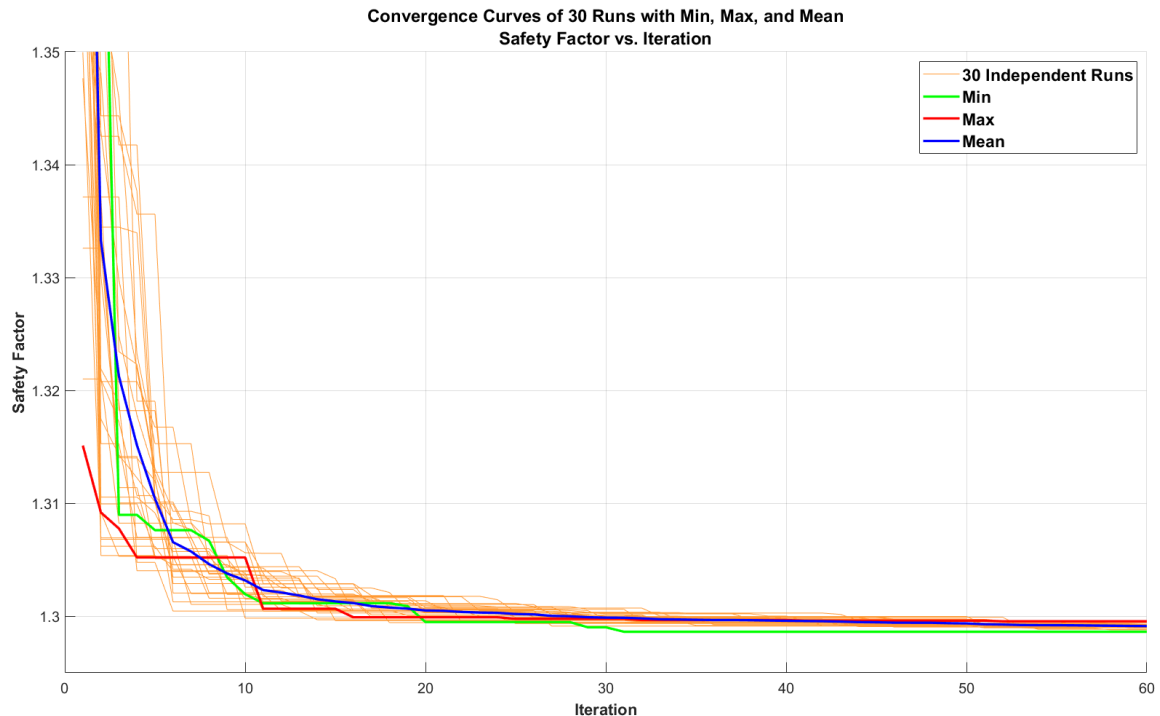


Figure 5: Convergence Curves for Benchmark Problem I (30 Runs)

The low standard deviation (0.000177) indicates high consistency across runs, suggesting that SA_EVPS reliably identifies the global minimum. The incorporation of seepage increased the FOS by approximately 5% compared to dry conditions, due to elevated pore pressures reducing effective stresses. The seismic coefficient further reduced the FOS by 3%, highlighting the destabilizing effect of dynamic loading. These results underscore SA_EVPS's ability to handle complex loading conditions effectively.

4.2 Benchmark Problem II

This benchmark problem, introduced by Zolfaghari et al. [9], is a more complex test case due to its steeper geometry and higher soil strength parameters, making it ideal for evaluating the robustness of optimization algorithms. The homogenous soil slope has the following properties:

- Effective cohesion: $c' = 14.71 \text{ kN/m}^2$,
- Friction angle: $\phi' = 20^\circ$,
- Unit weight: $\gamma = 18.63 \text{ kN/m}^3$,

The slope geometry, shown in Figure 6, has a height of 8 meters and an inclination angle of 25.20° . The horizontal extent from toe to crest is 25 meters. The water table is located 3 meters below the crest, contributing to seepage effects. A seismic coefficient of $k_h = 0.15$

was used to simulate a higher seismic intensity compared to Benchmark Problem I.

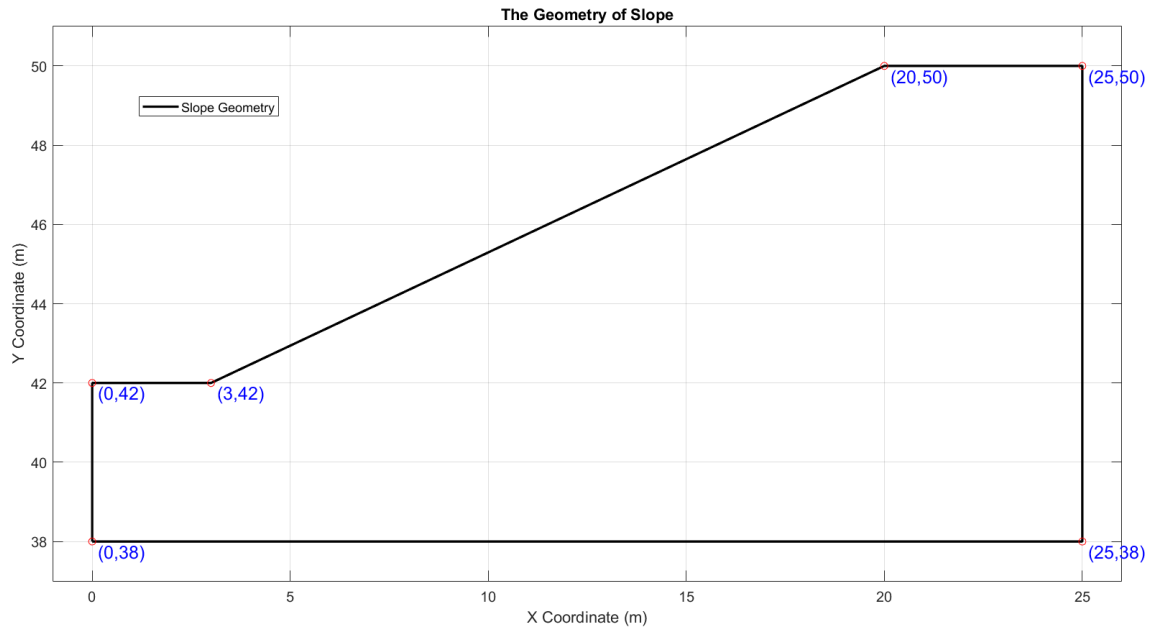


Figure 6: Geometry of Benchmark Problem II

The FEM analysis used a mesh of 600 three-node triangular elements, with boundary conditions specifying a fixed head of 12 meters on the upstream face and a seepage face on the downstream slope. The resulting pore pressure distribution was incorporated into the stability analysis.

The SA_EVPS algorithm was configured identically to Benchmark Problem I: 40 particles, 60 iterations, 30 runs, and 20 slices using FSDM. The search space was defined as $x_c \in [0, 25]$ m, $y_c \in [10, 70]$ m, and $R \in [10, 20]$ m.

Results are presented in Table 4, showing the best FOS, average FOS, and standard deviation.

Table 4: Statistical Results for Benchmark Problem II Using SA_EVPS

Benchmark 2	BHMO	FA	CMA-ES	ECM	SCA	Present study
Best	1.71E+00	1.72E+00	1.94E+00	1.84E+00	1.98E+00	1.7099
Average	1.72E+00	1.74E+00	1.98E+00	1.80E+00	2.10E+00	1.7118
Std.	1.92E-12	1.74E-01	3.55E-01	3.60E-01	4.71E-01	9.04E-04

The optimal CFS has $x_c = 7.606$ m, $y_c = 59.002$ m, and $R = 18.097$ m, yielding a minimum FOS of 1.7099. This FOS is lower than those reported by previous studies, indicating a more critical failure surface. The critical failure surface characteristics obtained from different optimization methods have been compared in Table 5. Comparisons with other methods are shown in Table 6. The critical failure surface is visualized in Figure 7,

showing its position relative to the slope geometry.

Table 5: Comparison of surface properties for Benchmark Problem II

CFS Properties	BHMO	EFA	CMA-ES	ECM	SCA	Present study
x Coordinate	7.4386	7.4184	7.4057	7.7538	7.3752	7.606
y Coordinate	59.0521	58.8634	58.8734	58.6321	58.5241	59.002
Radius	18.1049	17.8615	18.0298	17.6034	17.5943	18.097

Table 6: Comparison of FOS Values for Benchmark Problem II

Researcher	Method	Number of Slices	Limit Equilibrium Method	FOS
Zolfaghari et al. [9]	GA	-	Bishop's Method	1.7400
Zolfaghari et al. [9]	GA	-	Morgenstern Method	1.7600
Zolfaghari et al. [9]	GA	-	Morgenstern Method	1.7500
Cheng et al. [27]	PSO	40	Spencer's Method	1.7282
Kalatehjari et al. [10]	PSO	40	Bishop's Method	1.7197
Himanshu and Burman [28]	PSO	25	Bishop's Method	1.7218
Kaveh and Seddighian [29]	BHMO	20	Bishop's Method	1.7061
Kaveh and Seddighian [29]	EFA	20	Bishop's Method	1.7143
Kaveh and Seddighian [29]	CMA-ES	20	Bishop's Method	1.9436
Kaveh and Seddighian [29]	ECM	20	Bishop's Method	1.8401
Kaveh and Seddighian [29]	SCA	20	Bishop's Method	1.9834
Present study	SA_EVPS	20	Bishop's Method	1.7099

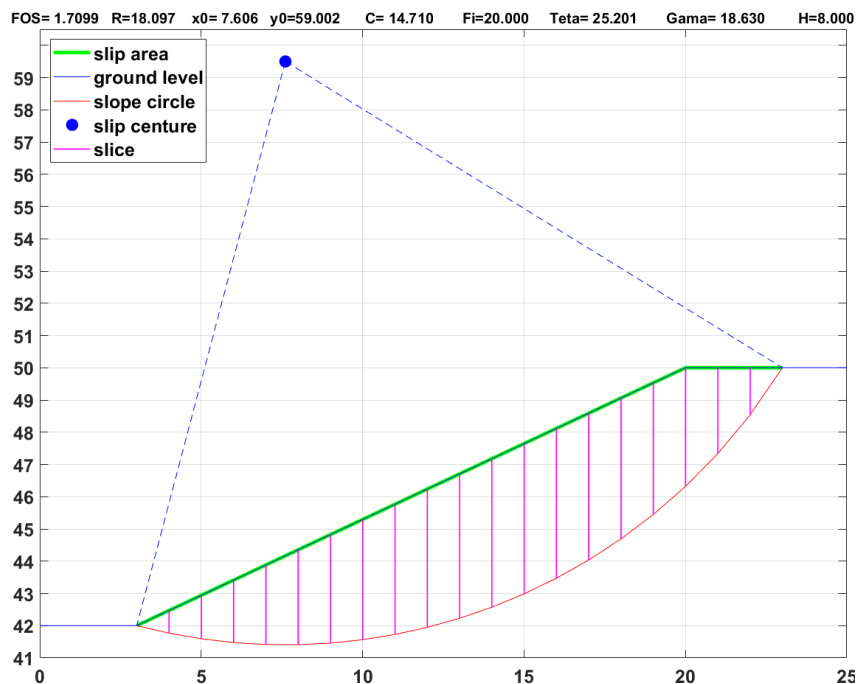


Figure 7: Critical Failure Surface for Benchmark Problem II

The Abaqus simulation, shown in Figure 8, illustrates stress contours along the optimized failure surface, with peak stresses aligning with the critical slip plane, validating the SA_EVPS results.

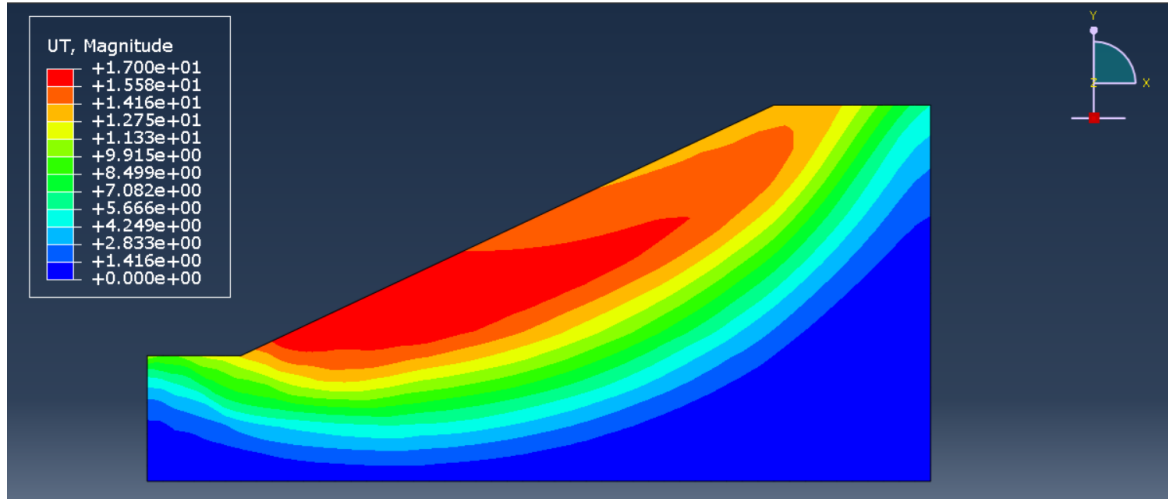


Figure 8: Abaqus Simulation of Optimized State for Benchmark Problem II

The convergence behavior is depicted in Figure 9, showing FOS values over iterations for the 30 runs. Convergence was achieved within approximately 45 iterations, with a standard deviation of 0.000904, indicating high consistency.

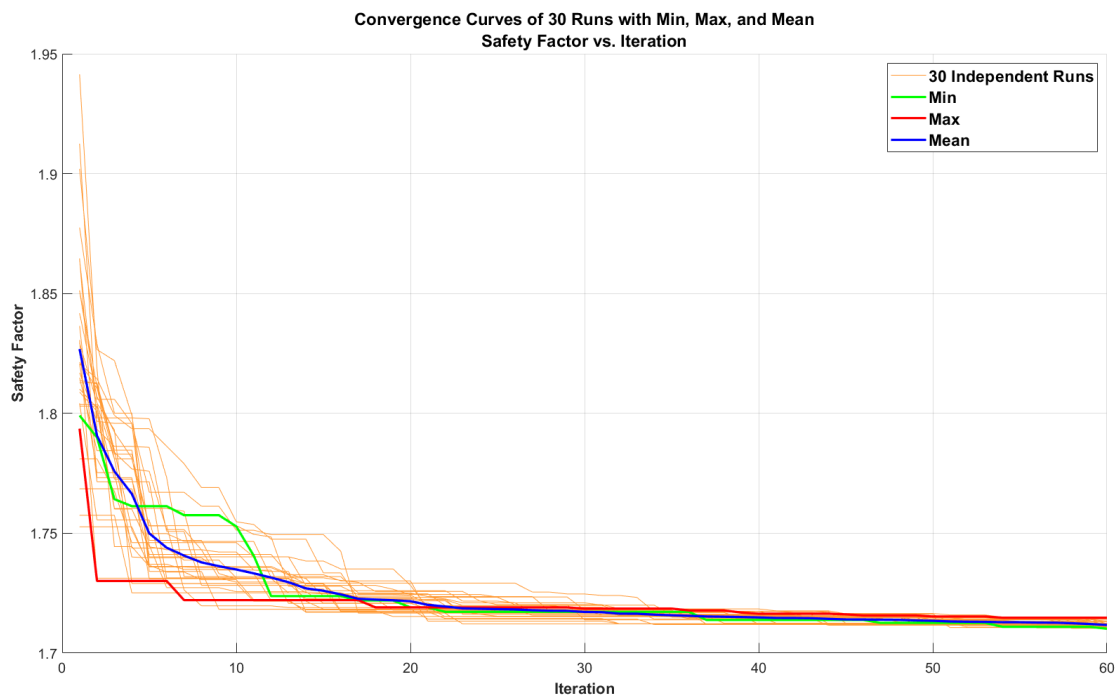


Figure 9: Convergence Curves for Benchmark Problem II (30 Runs)

Seepage effects increased the FOS by 4% compared to dry conditions, while the higher seismic coefficient reduced it by 5%, reflecting the combined impact of these factors. The steeper slope and higher soil strength in Benchmark Problem II posed a greater challenge, yet SA_EVPS consistently outperformed other methods, demonstrating its robustness.

5. DISCUSSION

The SA_EVPS algorithm demonstrated superior performance compared to both traditional and contemporary meta-heuristic methods across both benchmark problems. The algorithm achieved the lowest FOS values (1.2997 for Benchmark I and 1.7099 for Benchmark II) with remarkably small standard deviations (0.000177 and 0.000904, respectively), indicating exceptional accuracy and consistency.

The key advantage of SA_EVPS lies in its self-adaptive parameter optimization mechanism, which dynamically adjusts algorithm parameters to suit each specific problem [22]. This eliminates the need for manual parameter tuning, a significant limitation of conventional meta-heuristic algorithms. The integration of FEM provides accurate pore pressure distributions essential for realistic seepage modeling, while Bishop's simplified method offers an optimal balance between computational efficiency and accuracy.

Compared to PSO implementations [10] and GA approaches [9], SA_EVPS requires fewer discretization slices (20 versus 40) while achieving superior results. This computational efficiency is particularly valuable for large-scale geotechnical analyses. The Abaqus visualizations provide independent validation of the optimization results, with displacement and stress patterns aligning precisely with the identified critical failure surfaces.

However, several limitations should be acknowledged. The algorithm's performance may be sensitive to the initial parameter ranges, particularly for problems with highly irregular geometries. The computational complexity could increase significantly for three-dimensional analyses or non-homogeneous slopes with multiple soil layers. Additionally, the current implementation assumes circular failure surfaces, which may not capture all potential failure mechanisms in complex slopes.

Future research directions should explore extending SA_EVPS to non-circular failure surfaces, three-dimensional slope geometries, and time-dependent analyses incorporating rainfall infiltration and consolidation effects. Comparative studies with other self-adaptive algorithms would provide valuable insights into relative performance across diverse geotechnical applications.

6. CONCLUSION

This study successfully demonstrates the efficacy of the Self-Adaptive Enhanced Vibrating Particle System (SA_EVPS) algorithm in optimizing critical failure surfaces of homogeneous soil slopes under complex loading conditions. By integrating the Finite Element Method for accurate seepage modeling and Bishop's simplified method for stability analysis, the proposed approach provides a robust framework for geotechnical optimization.

The key contributions of this research include:

1. **Superior optimization performance:** SA_EVPS achieved minimum Factors of Safety of 1.2997 and 1.7099 for Benchmark Problems I and II respectively, outperforming all compared methods including Monte Carlo, Genetic Algorithm, and Particle Swarm Optimization approaches.
2. **Enhanced reliability:** The remarkably low standard deviations (0.000177 and 0.000904) across 30 independent runs demonstrate exceptional consistency, crucial for engineering applications where reliability is paramount.
3. **Self-adaptive capability:** The algorithm's ability to optimize its own parameters (α , p , w_1 , w_2 , HMCR, PAR, Neighbor, Memory_size) eliminates the need for problem-specific parameter tuning, enhancing its practical applicability.
4. **Comprehensive loading conditions:** The successful incorporation of both seepage and seismic effects through FEM integration provides more realistic stability assessments compared to simplified approaches.
5. **Computational efficiency:** Despite using fewer discretization slices than comparable methods, SA_EVPS achieved superior results with faster convergence (40-45 iterations), reducing computational costs for large-scale analyses.

The Abaqus finite element simulations provide independent validation of the optimization results, with stress and displacement patterns confirming the physical accuracy of the identified critical failure surfaces. The algorithm's robust performance across different slope geometries, soil properties, and loading conditions demonstrates its versatility for practical geotechnical applications.

While the current implementation focuses on circular failure surfaces in homogeneous slopes, the framework established in this study provides a solid foundation for future extensions. Potential developments include adaptation to non-circular failure surfaces, three-dimensional analyses, layered soil profiles, and time-dependent conditions incorporating rainfall infiltration and consolidation effects.

The SA_EVPS algorithm represents a significant advancement in geotechnical optimization, offering engineers a powerful tool for accurate and efficient slope stability analysis. Its self-adaptive nature, combined with proven superior performance, positions it as a valuable addition to the geotechnical engineering toolkit for addressing increasingly complex infrastructure challenges in seismically active regions with variable groundwater conditions.

REFERENCES

1. Fellenius W. Calculation of the stability of earth dams. In: *Proc 2nd Congr Large Dams*. 1936;4:445–63.
2. Bishop AW, Morgenstern NR. Stability coefficients for earth slopes. *Geotechnique*. 1960;10(4):129–50.
3. Morgenstern NR, Price VE. The analysis of the stability of general slip surfaces. *Geotechnique*. 1965;15(1):79–93.

4. Spencer E. A method of analysis of the stability of embankments assuming parallel inter-slice forces. *Geotechnique*. 1967;**17**(1):11–26.
5. Baker R, Garber M. Theoretical analysis of the stability of slopes. *Geotechnique*. 1978;**28**(4):395–411.
6. Chen ZY, Shao CM. Evaluation of minimum factor of safety in slope stability analysis. *Can Geotech J*. 1988;**25**(4):735–48.
7. Arai K, Tagyo K. Determination of noncircular slip surface giving the minimum factor of safety in slope stability analysis. *Soils Found*. 1985;**25**(1):43–51.
8. Kaveh A. *Advances in Metaheuristic Algorithms for Optimal Design of Structures*. Springer; 2017.
9. Zolfaghari AR, Heath AC, McCombie PF. Simple genetic algorithm search for critical non-circular failure surface in slope stability analysis. *Comput Geotech*. 2005;**32**(3):139–52.
10. Kalatehjari R, Ali NB, Ashrafi E. Finding the critical slip surface of a soil slope with the aid of particle swarm optimization. In: *Int Multidiscip Sci GeoConf SGEM*. 2011;**1**(1):459–66.
11. Yang XS. Firefly algorithms for multimodal optimization. In: *Int Symp Stoch Algorithms*. 2009:169–78.
12. Greco VR. Efficient Monte Carlo technique for locating critical slip surface. *J Geotech Eng*. 1996;**122**(7):517–25.
13. Paknahad M, Hosseini P, Kaveh A. A self-adaptive enhanced vibrating particle system algorithm for continuous optimization problems. *Int J Optim Civ Eng*. 2023;**13**(1):127–42.
14. Coello CAC, Lamont GB, Van Veldhuizen DA. *Evolutionary Algorithms for Solving Multi-Objective Problems*. Springer; 2007.
15. Kaveh A, Hoseini Vaez SR, Hosseini P, Bakhtiari M. Optimal design of steel curved roof frames by enhanced vibrating particles system algorithm. *Period Polytech Civ Eng*. 2019;**63**(4):947–60.
16. Paknahad M, Hosseini P, Kaveh A, Hakim SJS. A self-adaptive enhanced vibrating particle system algorithm for structural optimization: application to ISCSO benchmark problems. *Int J Optim Civ Eng*. 2025;**15**(1):111–30.
17. Hosseini P, Kaveh A, Naghian A, Abedi A. Optimization of artificial stone mix design using microsilica and artificial neural networks. *Int J Optim Civ Eng*. 2024;**14**(3):445–60.
18. Hosseini P, Kaveh A, Naghian A. Development and optimization of self-compacting concrete mixes: insights from artificial neural networks and computational approaches. *Int J Optim Civ Eng*. 2023;**13**(4):457–76.
19. Hosseini P, Kaveh A, Naghian A. The use of artificial neural networks and metaheuristic algorithms to optimize the compressive strength of concrete. *Int J Optim Civ Eng*. 2023;**13**(3):327–38.
20. Hosseini P, Kaveh A, Fathali MA, Hoseini Vaez SR. A two-loop RBDO approach for steel frame structures using EVPS, GWO, and Monte Carlo simulation. *Mech Adv Mater Struct*. 2024;**32**(4):605–24.
21. Malkawi AIH, Hassan WF, Sarma SK. Global search method for locating general slip surface using Monte Carlo techniques. *J Geotech Geoenviron Eng*. 2001;**127**(8):688–98.

22. Paknahad M, Hosseini P, Kaveh A. A self-adaptive enhanced vibrating particle system algorithm for continuous optimization problems. *Int J Optim Civ Eng*. 2023;**13**(1):127–42.
23. Haji Mazdarani MJ, Hoseini Vaez SR, Hosseini P, Fathali MA. Reliability-based layout optimization of concentrically braced in 3D steel frames. *Struct*. 2023;**47**:1094–1112.
24. Paknahad M, Mazaheri A, Alipour R. Examination the effect of soil parameters on earth dam slope stability in ABAQUS software. *J Hydraul Struct*. 2021;**7**(3):23–32.
25. Yamagami T, Ueta Y. Search for noncircular slip surfaces by the Morgenstern-Price method. In: *Proc 6th Int Conf Numer Methods Geomech*. 1988:1335–40.
26. Greco VR. Efficient Monte Carlo technique for locating critical slip surface. *J Geotech Eng*. 1996;**122**(7):517–25.
27. Cheng YM, Li L, Chi S, Wei WB. Particle swarm optimization algorithm for the location of the critical non-circular failure surface in two-dimensional slope stability analysis. *Comput Geotech*. 2007;**34**(2):92–103.
28. Himanshu N, Burman A. Determination of critical failure surface of slopes using particle swarm optimization technique considering seepage and seismic loading. *Geotech Geol Eng*. 2019;**37**(3):1261–81.
29. Kaveh A, Seddighian MR. Optimization of slope critical surfaces considering seepage and seismic effects using finite element method and five meta-heuristic algorithms. *Period Polytech Civ Eng*. 2021;**65**(2):425–36.